



The Impact of Bismuth Doping on the Mechanical, Optical, and Radiation-Shielding Properties of Borosilicate Glass Systems



CrossMark

Gharam A. Alharshan¹, Shaaban M. Shaaban², Mohamed Elsaifi³, R.A. Elsad^{4*}, Shima Ali Said⁵, A.M.A. Mahmoud⁵, A. Bahei El-Deen⁶, Asmae Mimouni⁷

¹Physics Department, College of Science, Princess Nourah Bint Abdulrahman University, P.O. Box 84428, Riyadh, 11671, Saudi Arabia

²Center for Scientific Research and Entrepreneurship, Northern Border University, Arar 73213, Saudi Arabia

³Physics Department, Faculty of Science, Alexandria University, Alexandria 21511, Egypt

⁴Basic Engineering Science Department, Faculty of Engineering, Menoufia University, 32511 Shebin El-Koom, Egypt

⁵Physics Department, Faculty of Science, AL Azhar University (Girls Branch), Cairo, Egypt

⁶Production Engineering & Mechanical Design Dept., Faculty of Engineering, Menoufia University, Shebin El-Kom, Minoufiya, Egypt.

⁷Department of Physics, College of Science, Imam Mohammad Ibn Saud Islamic University (IMSIU), P.O. Box 90950, Riyadh 11623, Saudi Arabia

Abstract

New glasses composed of 70B₂O₃ - 5SiO₂ - 10Li₂O - (5-x)PbO - 10ZnO - xBi₂O₃, with x = 0.0:5 mol%, were produced using the melt-quenching method. The density increased from 2.67 to 2.94 g/cm³ as 5 mol% of PbO was replaced with Bi₂O₃. The theoretical investigation and comparison with corresponding simulated findings generated from Geant4 simulation have been conducted for the attenuation characteristics of glasses coded from Bi-0.0 to Bi-5.0. As the quantity of Bi³⁺ ions in the glass's structure rises, the linear attenuation coefficient (LAC) values progressively rise for all applied energies. Half value layer (HVL) drops as Bi₂O₃ is substituted for PbO. The MFP values at 0.3 MeV were 2.667, 2.485, 2.326, 2.193, 2.090, and 2.005 cm for Bi-0.0, Bi-1.0, Bi-2.0, Bi-3.0, Bi-4.0, and Bi-5.0, respectively. Indirect optical gap (E_{OBG}) decreased from 3.072 V to 2.919 eV and direct optical band gap (E_{OBG}) varied from 3.359 eV to 3.170 eV as the amount of Bi³⁺ ions in the glass's structure increased. The Urbach energy value increases from 0.476 eV to 0.540 eV as the amount of Bi₂O₃ in the glass's lattice increases. Transmittance Coefficient (T), Molar Refraction (R_m), Molar Polarizability (α_m), and Optical Refractive Index are all estimated parameters that rise with increasing the amount of Bi₂O₃ in the glass's lattice. As the amount of Bi³⁺ ions increase in the glass's lattice, the Metallization Criterion, Optical Electronegativity (χ*), and Nonlinear Refractive Index (n₂) calculations show decreasing values. Mechanical moduli values grew steadily as PbO components were replaced with Bi₂O₃, reaching a glassy composite called Bi-3.0 before gradually declining once more. The glass system is recommended as a photon attenuation shielding material.

Keywords: linear attenuation coefficient; density; Urbach energy; optical band gap; Mechanical moduli.

1. Introduction

A form of radiation known as "ionizing radiation" is strong enough to ionize atoms by removing strongly bonded electrons from them. This phenomenon can result in a variety of biological and chemical effects on living things as well as materials. Ionizing radiation encompasses various forms of radiation, including beta and alpha particles, X-rays, and gamma rays. However, gamma-rays have a wide range of medical uses, including cancer therapy, whereas X-rays are frequently employed to photograph human tissue and diagnose injuries [1-3]. Because of the harmful impact radiation has on biological systems, protecting against artificial radiation sources as well as the level of natural radiation found in nature is an extremely essential topic that should never be neglected [4-6]. It is important to identify exactly the characteristics of radiation that are invisible to our senses, the ways in which it might interact with matter, and the possible scattering situations that can emerge from these interactions at various energy levels. Using specialized materials with proven and tested shielding qualities that are suitable for a given type of radiation makes radiation protection easier to carry out.

There are various forms of radiation shields, such as concretes, alloys, clays, glasses, and more [7-9]. Lead is another common material used as a radiation barrier [10-12]. Glass is one of these materials that has been utilized a lot in literature lately since it is inexpensive, easy to fabricate, and has the special quality of being transparent [13-16]. The main advantage

*Corresponding author e-mail: ragab.elsad@gmail.com; (Ragab A. Elsad).

Received date 18 February 2025; Revised date 12 April 2025; Accepted date 05 May 2025

DOI: [10.21608/EJCHEM.2025.361649.11325](https://doi.org/10.21608/EJCHEM.2025.361649.11325)

©2025 National Information and Documentation Center (NIDOC)

of borosilicate glasses over concrete materials is their exceptional radiation shielding behavior, which can be achieved by including metal oxides such as PbO, Bi₂O₃, ZnO, and BaO [17, 18]. Radiation blocking capacity is enhanced when a material has a greater atomic number because of a greater probability of photon interactions with the material [19]. Lead oxide glasses are traditionally considered the best radiation shielding materials due to their favorable physicochemical properties. On the other hand, alternative heavy metal oxide (Bi₂O₃) with a similar radiation shielding capacity has been produced in place of PbO, which is avoided due to its toxic nature [20].

This work examined the physical, mechanical, optical, and radiation shielding properties of borosilicate glasses doped with Li₂O, ZnO, and varied amounts of Bi₂O₃, and PbO.

2. Experimental

2.1 Preparation of samples







The melt-quenching method was used in the production process of glasses made of 70B₂O₃ - 5SiO₂ - 10Li₂O - (5-x)PbO - 10ZnO - xBi₂O₃, with $x = 0.0:5$ mol% and constant step, in order to ensure the highest level of perfection in the final product. An electronic scale with 0.001 g precision was used to balance the oxides at the beginning of the process, using the oxides with the highest AR grade. Various components have to be ground into tiny pieces with an agate mortar in order to produce a uniform mixture. After all the ingredients had been thoroughly combined, the crucible containing mixture was heated in a muffle furnace at 1100°C for one hour. After that, a steel mold was placed in an annealing furnace and heated to 300°C for the duration of the annealing process. The stainless steel mold was filled completely with the melted glass. This mold containing samples was annealed for three hour at 300°C. The goal of the annealing process is to reduce internal stress. After two hours, the ambient temperature was allowed to return to normal before the samples were carefully removed for further analysis. The photograph of synthesized specimens was given in Table 1.

The density values derived from the Archimedes principle and the subsequent formula are presented in Table 1 based on the following formula:

$$\rho_{\text{glass}} = \frac{W_{\text{Air}}}{(W_{\text{Air}} - W_{\text{Liquid}})} \times \rho_{\text{Liquid}} \quad (1)$$

where W_{Air} and W_{Liquid} refer to the sample weight in air and liquid, respectively (the used liquid was xylene, and its density is $\rho_{\text{Liquid}} = 0.863 \text{ g/cm}^3$).

Table 1: Samples code, glass composition, photograph, density, molar volume, oxygen packing density (OPD), and oxygen molar volume (OMV) of the prepared 70 B₂O₃-5 SiO₂-10Li₂O-(5-x) PbO-10ZnO -xBi₂O₃ with $x = 0.0, 1, 2, 3, 4$, and 5mol% glasses.

Sample code	Sample composition	Photograph of samples	Density, ρ (g.cm ⁻³)	molar volume	oxygen packing density, OPD	oxygen molar volume, OMV
Bi-0.0	70B ₂ O ₃ -5SiO ₂ -10Li ₂ O-5PbO -10ZnO		2.67	26.3221	96.87678	10.32239
Bi-1.0	70B ₂ O ₃ -5SiO ₂ -10Li ₂ O-4PbO -10ZnO-1Bi ₂ O ₃		2.74	26.5354	96.85175	10.32506
Bi-2.0	70B ₂ O ₃ -5SiO ₂ -10Li ₂ O-3PbO -10ZnO-2Bi ₂ O ₃		2.81	26.73808	96.8656	10.32358
Bi-3.0	70B ₂ O ₃ -5SiO ₂ -10Li ₂ O-2PbO -10ZnO-3Bi ₂ O ₃		2.87	27.02474	96.57818	10.35431
Bi-4.0	70B ₂ O ₃ -5SiO ₂ -10Li ₂ O-1PbO -10ZnO-4Bi ₂ O ₃		2.91	27.48729	95.6806	10.45144
Bi-5.0	70B ₂ O ₃ -5SiO ₂ -10Li ₂ O-10ZnO-5Bi ₂ O ₃		2.94	28.03231	94.53376	10.57823

3. Result and discussion

3.1 Physical properties

Table 1 and Fig. 1 demonstrate that sample density increases as bismuth content increases. The main reason for this increase is that the lighter PbO molecules ($M=223.2$ g/mol) have been replaced by denser Bi_2O_3 molecules ($M= 465.96$ g/mol). There is a structural change caused by the addition of heavier Bi^{3+} ions to the glass network because there are many oxygen ions available in the structure. The following relation can be used to determine the molar volume, which provides an image of the interstitial space found in the glass structure:

$$V_m = \frac{M_{\text{Wglass}}}{\rho_{\text{glass}}} \quad (2)$$

where M_{Wglass} is the glass's molecular weight.

Table 1 and Figure 1 also display the computed molar volume (V_m) values. When more Bi_2O_3 is added to the glass samples, their molar volume increases. This is because the bond lengths of Bi_2O_3 (ranging from 2.16 to 2.79 Å) [21] have larger radii than those of PbO (ranging from 2.34 to 2.37 Å) [22], which results in more free volume in the glass network. As a result, the glass structure becomes less densely packed and more open as non-bridging oxygen's (NBOs) form [23, 24].

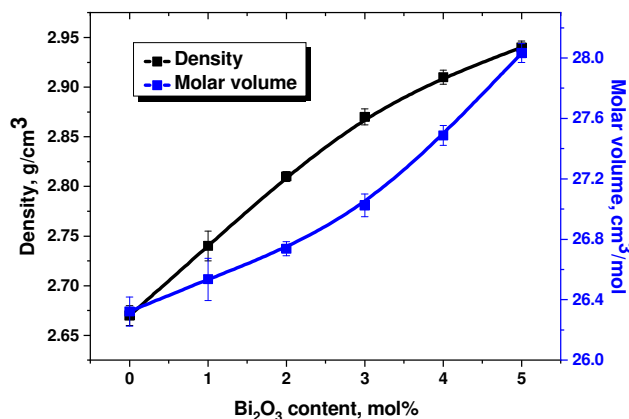


Figure 1: Variation of density and molar volume of glass samples as a function of Bi_2O_3 molar content.

The dependence of oxygen packing density (OPD) and oxygen molar volume (OMV) on Bi-ions percent is shown in Table 1 and Fig. 2. When Bi_2O_3 is gradually added to the prepared glasses, OPD values first appear to alter slightly before quickly declining, indicating a development in non-bridging oxygen (NBO) atoms within the glass's internal molecular structure [25]. The OMV value increased in opposite trend with OPD value. This behavior can be explained based on the dual role of Bi_2O_3 acting both as network modifier initially and then as network former due to its higher concentration [26].

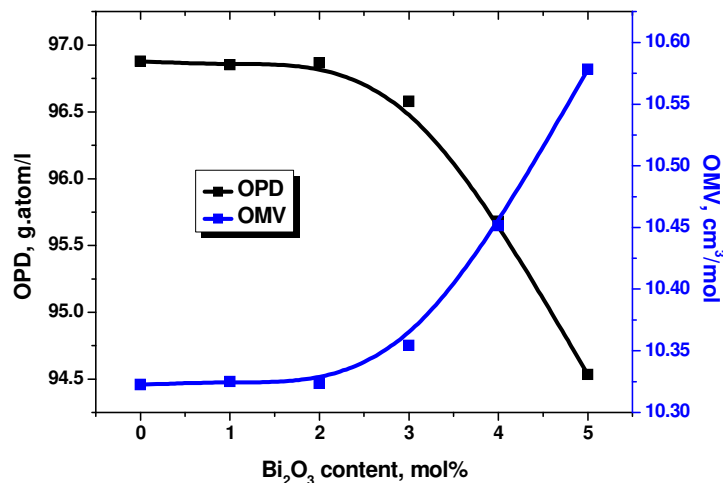


Figure 2: Oxygen molar volume (OMV) and oxygen packing density (OPD) as a function of Bi_2O_3 molar percent in the glass samples.

3.2 Shielding characteristics

The attenuation parameters of glasses coded from Bi-0.0 to Bi-5.0 have been investigated theoretically using Phy-x software [27], and compared with corresponding simulated results obtained from Geant4 simulation [28, 29]. The linear attenuation coefficient or LAC represents the absorption and scattering probability through path length of absorbed material. Table.2 shows the values of two results from 0.03 to 15 MeV and the deviation (Dev, %) of each two corresponding values for

discussed glass samples. The maximum deviation (M.D) observed between the two software was 2.75% for the Bi-2.0 sample at 5 MeV, and this is evidence of the extent to which the results match despite the difference in samples and energies. The M.D of Bi-0.0 was 2.11% at 0.30 MeV, the M.D of Bi-1.0 was 2.11% at 4.0 MeV, the M.D of Bi-3.0 was 2.01% at 4.0 MeV, the M.D of Bi-4.0 was 1.83% at 0.03 MeV and the M.D of Bi-5.0 was 1.80% at 0.10 MeV. One of the characteristics of the LAC its value decreases with the increase in energy falling on the material, and this is consistent with Table 2. For example, sample B-2.0 has 26.343 cm^{-1} at lowest discussed energy (0.03 MeV), while has 0.085 cm^{-1} at highest discussed energy (15.0 MeV). With the amount of PbO gradually replaced from 0 to 5 mol% by Bi_2O_3 , the LAC values gradually increases for all applied energies and the values of Bi-5.0> Bi-4.0> Bi-3.0> Bi-2.0> Bi-1.0> Bi-0.0 and that is clear in Fig.3.

Table 2: The LAC values at different energies by the Phy-x software and Geant4 simulation results in addition, the relative deviation between them.

LAC, cm^{-1}											
Bi-0.0				Bi-1.0				Bi-2.0			
Energy, MeV	Phy-x	Geant4	Dev, %	Energy, MeV	Phy-x	Geant4	Dev, %	Energy, MeV	Phy-x	Geant4	Dev, %
0.03	16.920	16.751	1.01	0.03	18.952	18.644	1.65	0.03	26.343	25.970	1.44
0.04	7.941	7.876	0.82	0.04	8.907	8.821	0.98	0.04	12.425	12.275	1.22
0.05	4.489	4.449	0.91	0.05	5.031	4.997	0.69	0.05	7.005	6.936	1.00
0.06	2.873	2.905	-1.11	0.06	3.213	3.154	1.88	0.06	4.446	4.417	0.67
0.08	1.509	1.517	-0.54	0.08	1.673	1.640	2.02	0.08	2.266	2.252	0.63
0.10	2.255	2.252	0.11	0.10	2.624	2.577	1.85	0.10	3.990	3.956	0.86
0.15	0.988	0.976	1.26	0.15	1.123	1.108	1.32	0.15	1.616	1.591	1.58
0.20	0.614	0.604	1.64	0.20	0.681	0.674	1.09	0.20	0.925	0.914	1.21
0.30	0.375	0.367	2.11	0.30	0.402	0.400	0.67	0.30	0.499	0.494	0.99
0.40	0.292	0.289	1.22	0.40	0.308	0.311	-0.78	0.40	0.362	0.360	0.78
0.50	0.250	0.249	0.27	0.50	0.261	0.258	1.30	0.50	0.298	0.301	-0.97
0.60	0.223	0.221	0.72	0.60	0.231	0.235	-1.67	0.60	0.259	0.264	-1.88
0.80	0.189	0.190	-0.88	0.80	0.195	0.195	-0.11	0.80	0.214	0.211	1.57
1.00	0.167	0.164	1.65	1.00	0.172	0.174	-1.22	1.00	0.187	0.185	1.11
1.50	0.134	0.132	1.03	1.50	0.138	0.136	1.08	1.50	0.148	0.148	0.07
2.00	0.116	0.116	0.33	2.00	0.119	0.117	1.86	2.00	0.129	0.127	1.48
3.00	0.096	0.096	0.82	3.00	0.099	0.097	2.06	3.00	0.108	0.108	0.40
4.00	0.086	0.085	0.73	4.00	0.089	0.087	2.11	4.00	0.098	0.096	1.68
5.00	0.080	0.079	1.82	5.00	0.083	0.082	1.58	5.00	0.092	0.090	2.75
6.00	0.076	0.075	0.83	6.00	0.079	0.078	1.22	6.00	0.089	0.087	1.28
8.00	0.072	0.071	0.99	8.00	0.075	0.074	1.94	8.00	0.085	0.084	0.94
10.00	0.070	0.069	1.93	10.00	0.073	0.072	1.08	10.00	0.084	0.083	1.92
15.00	0.069	0.068	1.72	15.00	0.073	0.072	0.68	15.00	0.085	0.085	1.07
Bi-3.0				Bi-4.0				Bi-5.0			
Energy, MeV	Phy-x	Geant4	Dev, %	Energy, MeV	Phy-x	Geant4	Dev, %	Energy, MeV	Phy-x	Geant4	Dev, %
0.03	22.930	22.517	1.83	0.03	24.696	24.253	1.83	0.03	24.696	24.661	0.14
0.04	10.799	10.615	1.73	0.04	11.640	11.442	1.73	0.04	11.640	11.516	1.08
0.05	6.093	5.996	1.62	0.05	6.565	6.487	1.20	0.05	6.565	6.675	-1.64
0.06	3.877	3.826	1.33	0.06	4.172	4.133	0.93	0.06	4.172	4.201	-0.70
0.08	1.994	1.956	1.92	0.08	2.135	2.106	1.38	0.08	2.135	2.146	-0.49
0.10	3.351	3.294	1.73	0.10	3.680	3.634	1.27	0.10	3.680	3.615	1.80
0.15	1.387	1.373	0.98	0.15	1.505	1.526	-1.38	0.15	1.505	1.483	1.53
0.20	0.813	0.807	0.74	0.20	0.871	0.879	-0.91	0.20	0.871	0.859	1.35
0.30	0.456	0.465	-1.99	0.30	0.478	0.485	-1.38	0.30	0.478	0.472	1.32
0.40	0.339	0.341	-0.64	0.40	0.351	0.346	1.49	0.40	0.351	0.351	0.07
0.50	0.282	0.279	1.38	0.50	0.291	0.288	1.02	0.50	0.291	0.287	1.34
0.60	0.248	0.246	0.74	0.60	0.254	0.252	0.93	0.60	0.254	0.252	0.95

0.80	0.207	0.205	0.64	0.80	0.211	0.207	1.87	0.80	0.211	0.210	0.58
1.00	0.181	0.178	1.85	1.00	0.184	0.186	-0.78	1.00	0.184	0.182	0.97
1.50	0.145	0.142	1.85	1.50	0.147	0.147	-0.19	1.50	0.147	0.145	1.32
2.00	0.125	0.124	0.85	2.00	0.127	0.126	1.04	2.00	0.127	0.126	0.96
3.00	0.105	0.103	1.74	3.00	0.107	0.105	1.25	3.00	0.107	0.107	-0.49
4.00	0.094	0.093	2.01	4.00	0.096	0.095	0.97	4.00	0.096	0.095	1.45
5.00	0.088	0.087	1.63	5.00	0.090	0.090	0.73	5.00	0.090	0.091	-0.99
6.00	0.085	0.084	0.64	6.00	0.087	0.086	1.10	6.00	0.087	0.086	1.43
8.00	0.081	0.080	1.64	8.00	0.083	0.082	1.62	8.00	0.083	0.082	1.21
10.00	0.080	0.079	1.03	10.00	0.082	0.081	0.92	10.00	0.082	0.081	1.23
15.00	0.069	0.069	0.74	15.00	0.083	0.084	-0.76	15.00	0.083	0.083	0.44

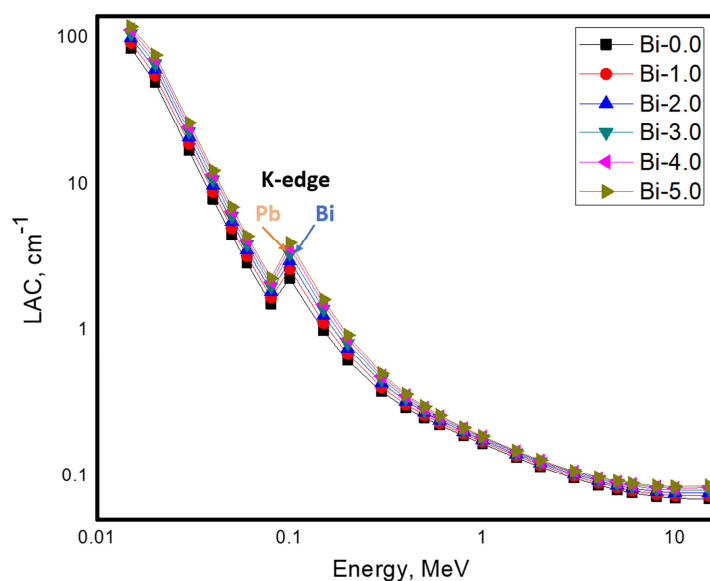


Figure 3: The LAC of Bi-x.0 glass composites at different variety of energies (x=0,1,2,3,4 and 5).

The absorption peak formed by the nearly total absorption of energies 80 and 81 keV within the absorbing material is shown in Fig. 3 and indicates that the k-edges of Pb and Bi are important in the attenuation process. This peak also has an impact on the rest of the energies. Due to the dominance of the photoelectric reaction at low energies (the probability of complete absorption of the incident photons), the LAC values were as high as possible. However, as the energy increased, the effect of the photoelectric interaction also decreased and the effect of Compton scattering (i.e., the probability of scattering increased) appeared [30,31]. The pair production effect (the possibility of the incident photons escaping increases) starts to emerge when the Compton scattering effect gradually increases, reaching an energy of 1.02 MeV. This causes the LAC values to fall as indicated in Fig. 4.

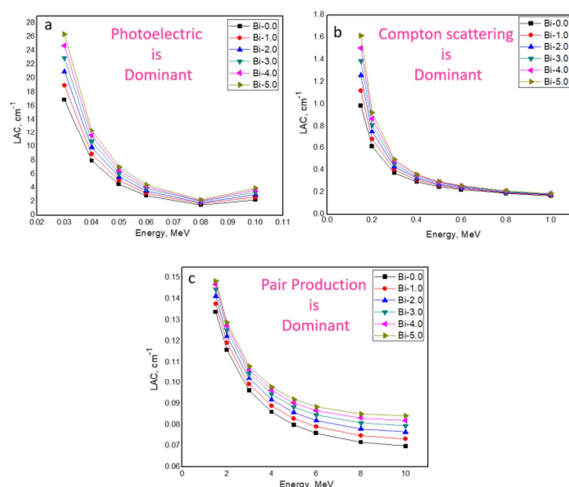


Figure 4: The LAC values at different energies, a) from 0.03 to 0.1 MeV, b) from 0.15 to 1 MeV and c) from 1.5 to 10 MeV.

Subtracting the density from the linear attenuation coefficient yields the mass attenuation coefficient, which is the attenuation of the material without the impact of density. Fig.5 shows the MAC of present glasses from 0.015 to 15 MeV. The variation of MAC with gamma-ray energy showed the same behavior. For example, at 0.3 MeV (300 keV), the values of MAC were 0.140, 0.147, 0.153, 0.159, 0.164, and 0.170 $\text{cm}^2 \text{g}^{-1}$ for Bi-0.0, Bi-1.0, Bi-2.0, Bi-3.0, Bi-4.0, and Bi-5.0, respectively. This indicates that the MAC values increased when PbO was replaced with Bi_2O_3 . At high energies from 1.0 MeV and above, the MAC values stay constant for all studied glasses. In glasses at 3.0 MeV, we find that the MAC value is constant and does not change when Bi_2O_3 is substituted for PbO. This is approximately equivalent to $0.050 \text{ cm}^2 \text{g}^{-1}$ due to their k-edges are almost identical.

The thickness, or HVL, as a function of energy required to reduce the gamma-line intensity to half of its starting value is plotted in Figure 6. This thickness rises gradually with the increase of the applied energy for all the glass studied. However, when PbO is replaced with Bi_2O_3 , as shown in Fig. 6, this thickness decreases. The HVL at low energies such as 0.06 MeV was 0.241, 0.216, 0.195, 0.179, 0.166 and 0.156 cm for Bi-0.0, Bi-1.0, Bi-2.0, Bi-3.0, Bi-4.0 and Bi-5.0, respectively. The HVL at intermediate energies such as 0.60 MeV was 3.113, 2.996, 2.886, 2.795, 2.727 and 2.673 cm for Bi-0.0, Bi-1.0, Bi-2.0, Bi-3.0, Bi-4.0 and Bi-5.0, respectively, while at high energies such as 2 MeV was 5.979, 5.815, 5.659, 5.531, 5.445 and 5.381 cm, respectively. From an environmental perspective, it is necessary to lower the PbO content and create a glass material with a higher attenuation because lead is known to be hazardous to both the environment and human health.

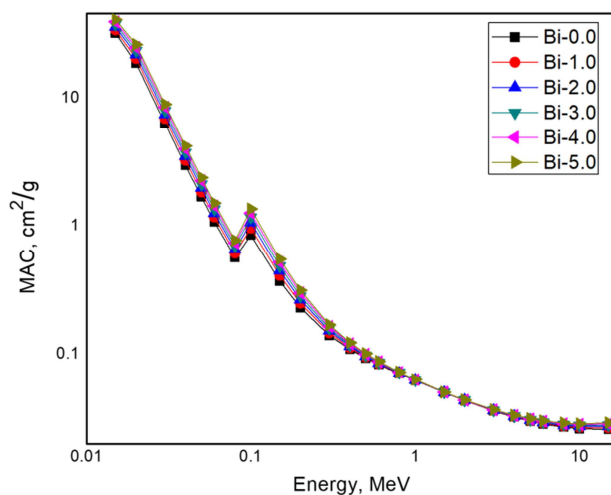


Figure 5: The MAC of present Bi-glass composites from 0.015 to 15 MeV.

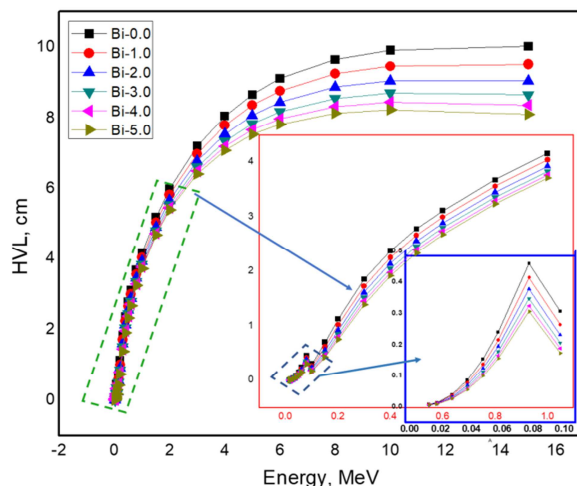


Figure 6: The HVL of present Bi-glass composites from 0.015 to 15 MeV.

As seen in Fig. 7, the MFP of the glass composites ranging from Bi-0.0 to Bi-5.0 was evaluated at various energies. In general, when photon energy increased, the MFP was enhanced. MFP was decreased from 0.012 cm for the Bi-0.0 to 0.008 cm for the Bi-5.0 sample at 0.015 MeV and from 0.663 cm for the Bi-0.0 to 0.441 cm for the Bi-5.0 sample at 0.08 MeV. The MFP values for Bi-0.0, Bi-1.0, Bi-2.0, Bi-3.0, Bi-4.0, and Bi-5.0 at energy of 0.3 MeV were 2.667, 2.485, 2.326, 2.193, 2.090, and 2.005 cm, respectively. Also, the average path distance traveled by a 1 MeV photon between two successive collisions was 6.003, 5.826, 5.660, 5.521, 5.427 and 5.354 cm for Bi-0.0, Bi-1.0, Bi-2.0, Bi-3.0, Bi-4.0 and Bi-5.0, respectively.

In Figure 8, the tenth thickness layer, or TVL, or the thickness needed to lower the gamma-line intensity to 90% of its initial value, was shown against photon energy. As observed in Fig. 8, this thickness steadily increases as the applied energy for all the glass under study increases. However, this thickness reduces when PbO is replaced with Bi₂O₃. The TVL at low energies has great data: for Bi-0.0, Bi-1.0, Bi-2.0, Bi-3.0, Bi-4.0, and Bi-5.0, the values at 0.05 MeV were 0.513, 0.458, 0.413, 0.378, 0.351, and 0.329 cm, respectively. This means that the lowest thickness required to reduce the photon intensity to 90% of its starting value is approximately 3.30 mm. The TVL increased at intermediate energies because of the increased probability of photon interaction. For instance, for Bi-0.0, Bi-1.0, Bi-2.0, Bi-3.0, Bi-4.0, and Bi-5.0, the TVL at 0.50 MeV was 9.224, 8.826, 8.462, 8.155, 7.924 and 7.735 cm, respectively, while at high energies like 1 MeV, it was 13.823, 13.416, 13.032, 12.496, and 12.329 cm, respectively.

The present results were compared with different commercial glasses [32] and other published work [33] related to this study as reported in Table 3. The comparison shown in Table 3 shows that the glass system studied in this paper represents an alternative to previously published and applied glass types such as RS-253-G18 and NB-BaO and is applicable as transparent shielding materials.

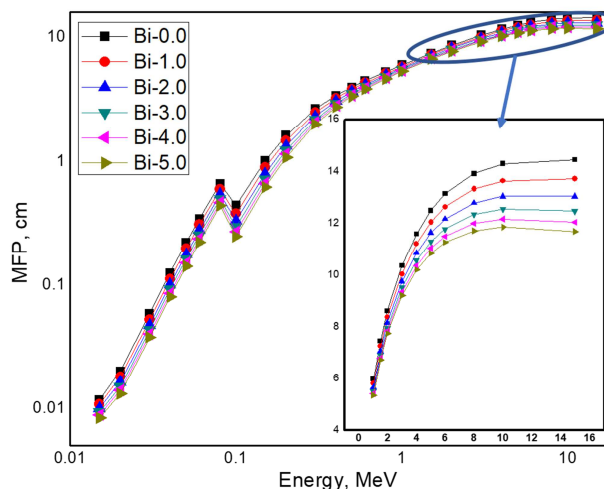


Figure 7: The MFP of present Bi-glass composites from 0.015 to 15 MeV.

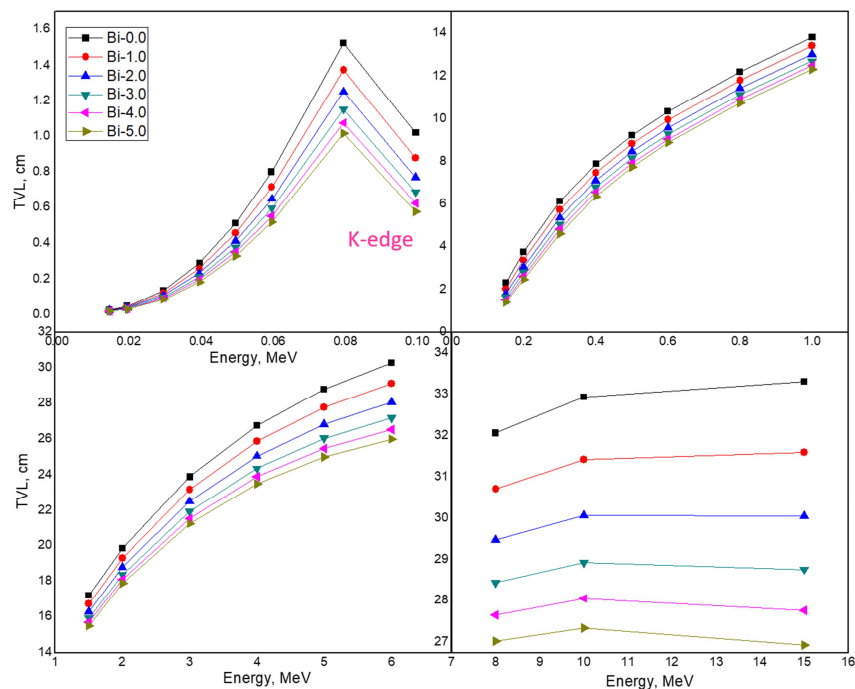


Figure 8: The TVL of present Bi-glass composites from 0.015 to 15 MeV.

Table 3: Comparison of the attenuation coefficient of the studied samples with other published and commercial samples

References	Glass code	LAC, cm^{-1}			HVL, cm		
		0.1 MeV	0.6 MeV	1.5 MeV	0.1 MeV	0.6 MeV	1.5 MeV
Commercial glasses [32]	RS-253-G18	0.580	0.203	0.130	1.194	3.408	5.334
	RS-360	8.704	0.356	0.187	0.080	1.946	3.712
Published work [33]	NB-MoO ₃	1.076	0.229	0.145	0.644	3.027	4.784
	NB-BaO	2.482	0.246	0.150	0.279	2.822	4.627
	NB-ZnO	0.601	0.218	0.140	1.153	3.178	4.967
Present work	Bi-0.0	2.255	0.223	0.134	0.307	3.113	5.178
	Bi-1.0	2.624	0.231	0.138	0.264	2.996	5.038
	Bi-2.0	3.990	0.259	0.148	0.174	2.673	4.668
	Bi-3.0	3.351	0.248	0.145	0.207	2.795	4.795
	Bi-4.0	3.680	0.254	0.147	0.188	2.727	4.723
	Bi-5.0	3.680	0.254	0.147	0.188	2.727	4.723

3.3 Optical properties

Figure 9 displays the UV-Vis-NIR absorbance spectra of the produced samples. The absorbance increases significantly as the percentage of Bi^{3+} ions increased, and the absorption edge shifted towards a higher wavelength. All specimens exhibited strong absorption peaks in the UV region from 200 to 400 nm, after 400 nm there is no absorption peaks for all the sample in the visible and NIR zones indicating their high transparency. The changes in the inner structures of the resulting glass block networks is consistent with the red color shift in the absorbing edge toward higher wavelengths as the concentration of Bi^{3+} ions increased.

As seen in Figure 10, the primary absorbing edge of the sample glasses' optical absorption coefficient (α) is situated in the area between 3.3 and 3.65 eV. We notice that a rise in Bi^{3+} ions result in a rise in (α) and shifting in the absorption edge towards lower photon energy. Energy band gap of glass materials (E_{OBG}) has importance for determining their optical

applications. Also, variations in the optical gap values are linked to the structural alterations based on the stoichiometry [34-36]. Based on Davis-Mott relation the energy gap can be assessed as [37,38]:

$$(\alpha h\nu)^n = B (h\nu - E_{\text{OBG}}) \quad (3)$$

Where E_{OBG} is the optical band gap energy, B is a constant and n have values 1/2, 2, 3, and 3/2 based upon the inter-band electronic transition.

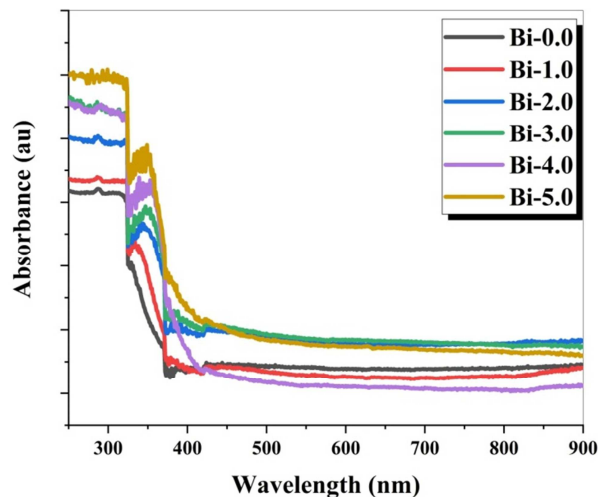


Figure 9: Displaying of the UV-Vis-NIR absorbance spectra of the glass samples

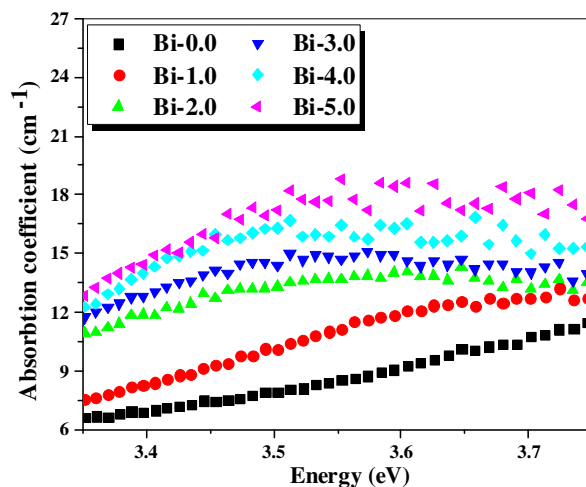


Figure 10: The variation of absorption coefficient (α) for glasses treated with varying amounts of Bi_2O_3 with photon energy.

The band gap energies for all the samples are found in Figs. 11 and 12 by plotting $(\alpha h\nu)^{1/2}$ and $(\alpha h\nu)^2$ against the photon energy at $(\alpha h\nu)^{1/2} = 0$ and $(\alpha h\nu)^2 = 0$, where the linear portions are extrapolated to the x-axis for estimating the values of the direct and indirect optical band gaps, which are listed in Table 4. The values of the indirectly and directly band gaps decrease when the percentage of Bi^{3+} increase from 0.0 to 5.0 mol%. The decrease in the energy gap of the bandwidth ranges from 5.306 eV for specimen Bi-0.0 to 5.027 eV for specimen Bi-5.0 for direct transitions and ranges from 5.096 eV for specimen Bi-0.0 to 4.651 eV for specimen Bi-5.0 for indirect transitions. Increasing Bi^{3+} ions cause this red-shift in the absorption edge due to internal structural changes [39].

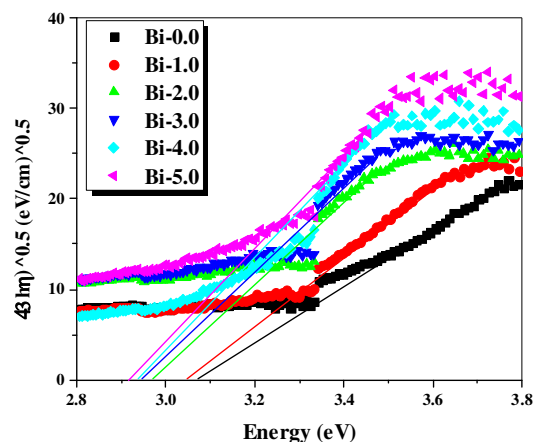


Figure 11: Plot of $(\alpha h\nu)^{1/2}$ against $h\nu$ (Tauc's plot) for the prepared glass samples.

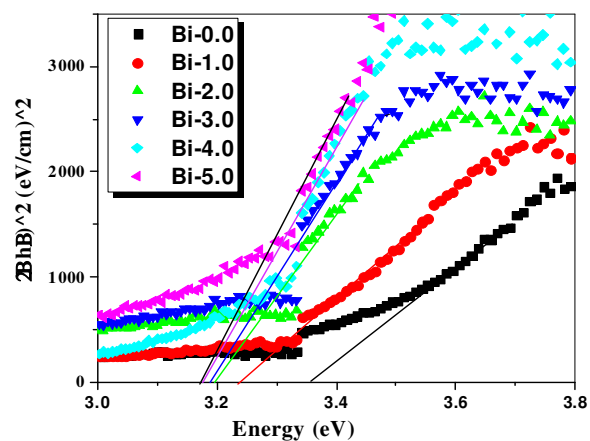


Figure 12: Plot of $(\alpha h\nu)^2$ against $h\nu$ (Tauc's plot) for the prepared glass samples.

Table 4: Optical parameters of the borosilicate glass doped with Bi_2O_3 .

Parameters	Sample code					
	Bi-0.0	Bi-1.0	Bi-2.0	Bi-3.0	Bi-4.0	Bi-5.0
Direct bandgap (eV)	3.359	3.236	3.196	3.192	3.178	3.170
Indirect bandgap (eV)	3.072	3.049	2.971	2.945	2.935	2.919
Urbach Energy(E_U)	0.476	0.487	0.501	0.513	0.526	0.540
Refractive index(n)	2.306	2.336	2.345	2.347	2.350	2.352
Molar refraction (R_m)	15.535	15.862	16.049	16.228	16.530	16.872
Molar polarizability (α_m) $\times 10^{-24}$	6.162	6.291	6.366	6.437	6.556	6.692
Electronic polarizability(α_e) $\times 10^{-25}$	3.340	3.370	3.80	3.381	3.385	3.387
Reflection loss (R_L)	0.156141	0.160423	0.161852	0.161996	0.162501	0.162791
Transmittance coefficient (T)	0.729893	0.723509	0.721389	0.721176	0.720428	0.719999
Metallization Criterion (M (E_g))	0.409	0.402	0.3998	0.3995	0.3986	0.3981
Metallization Criterion (M(n))	0.409	0.402	0.3998	0.3995	0.3986	0.3981
the permittivity(ϵ)	5.320	5.458	5.504	5.509	5.525	5.535
the optical dielectric constant (ϵ')	4.320	4.458	4.504	4.509	4.525	4.535
Optical electronegativity (χ^*)	9.028	8.698	8.591	8.580	8.542	8.520
linear dielectric susceptibility ($\chi^{(1)}$)	0.343	0.354	0.3586	0.3590	0.3603	0.3610
third-order nonlinear optical susceptibility ($\chi^{(3)}$) $\times 10^{-15}$	2.343	2.142	2.079	2.073	2.052	2.039
nonlinear refractive index (n_2) $\times 10^{-15}$	6.381	5.759	5.567	5.548	5.482	5.445

The link between the optical energy ($h\nu$) and the optical absorption coefficient (α) at lower photon energies is provided by Urbach's function. The Urbach energy, or E_U , can be computed [40] using the following formula:

$$\ln \alpha = \ln \alpha_0 + \frac{h\nu}{E_U} \quad (4)$$

Where E_U represent the band tail width and α_0 is a constant. E_U values derived from the inverse value of the slope obtained from the graphs of $\ln(\alpha)$ against ($h\nu$) (shown in Fig. 13). The Urbach energy (E_U) values (shown in Table 4) were found to rise from 0.448 eV to 0.668 eV with changes in the mol.% of Bi^{3+} ions, this is consistent with the value discovered for amorphous semiconductors (0.046 – 0.66 eV). The rise in calculated Urbach energy caused by increasing the amount of Bi_2O_3 is attributed to defecting in structural of the resulting glass block networks, also it an indication of the evolution of structural distortions in the examined glasses.

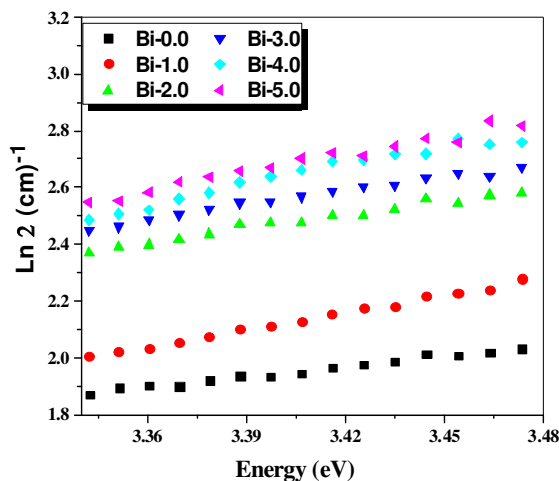


Figure 13: Plot of ($\ln \alpha$) against $h\nu$ for the prepared glass samples under examination

The refractive index (n) that illustrates the interactions between electromagnetic radiations with various materials can be calculated according to the Dimitrov and Sakka formula by using the optical energy gap, E_g , [41]:

$$\frac{n^2-1}{n^2+2} = 1 - \sqrt{\frac{E_g}{20}} \quad (5)$$

The refractive index of the borosilicate glasses (values of n are presented in table 4) was enhanced from 2.306 to 2.352 with increasing of Bi_2O_3 content from 0 to 5.0 mol%. Non-bridging oxygen bonds are created when Bi_2O_3 is incorporated into the glass network as a modifier. These non-bridging oxygen ions have a high polarizability, which raises the refractive index [42]. The following formulas were used to determine the molar refractivity (R_m), molar polarizability (α_m), and electronic polarizability (α_e):[43-45]

$$R_m = \left[\frac{n^2-1}{n^2+2} \right] V_m \quad (6)$$

$$\alpha_m = \frac{3x R_m}{4x \pi N_A} \quad (7)$$

$$\alpha_e = \frac{3(n^2-1)}{4\pi N_A(n^2+2)} \quad (8)$$

where N_A is Avogadro's number and V_m is the volume of a molar (Table 4 shows the values of R_m , α_m , and α_e). The exact relationship between molar polarizability and molar refraction can be seen in the Lorentz-Lorentz relation, which represents the number of electrons corresponding to the applied field. The increase in molar polarizability and molar reflectivity values can be linked to the quantity of non-bridging oxygen molecules because the rising NBO provides a substantial number of extra oxygen molecules to the glass network, boosting molar polarizability [42]. We note the values of α_e are increased by enhancement the percentage of Bi_2O_3 content in the glass network.

The reflection loss (R_L) and transmission coefficient (T) values of all the prepared glass samples are listed in Table 4 and computed [43,46] accordance with the following relations:

$$R_L = \left(\frac{n-1}{n+1} \right)^2 \quad (9)$$

$$T = \frac{2n}{n^2+1} \quad (10)$$

By increasing Bi_2O_3 content each of the reflection loss values and transmission coefficient values increase, this increment is correlated to the increasing in the refractive index values, in which a higher refractive increases the Fresnel reflection loss at the interface of the glass. We note that, the changes in R_L are relatively small, implying that, borosilicate glasses with doped Bi_2O_3 remain good optical transparency as we see from the higher values of transmittance coefficient (T). The observed increase in refractive index and reflection loss with Bi_2O_3 doping are consistent with the modifier role of Bismuth oxide in the glass lattice [42].

The optical energy-based metallization criteria ($M(E_g)$) given from the relation: [47]

$$M(E_g) = \sqrt{\frac{E_g}{20}} \quad (11)$$

While the metallization criterion ($M(n)$) based on refractive index can be obtained using [47] the following formula

$$M(n) = 1 - \left\{ \frac{n^2 - 1}{n^2 + 2} \right\} \quad (12)$$

Metallization Criterion (M) demonstrates both the metallic and nonmetallic character of the substance values of Bi_2O_3 -doped borosilicate glasses, when M approaches approximate value 1 the material exhibits roughly an insulator behavior, and when M approaches approximate value 0 exhibits a metallic behavior [48]. As we see from the values of (M) as listed in Table 4, the addition of Bi_2O_3 reduced $M(E_g)$ and $M(n)$ values in the present glass samples from 0.409 to 0.398.

Depending on the values of the refractive index each of the permittivity (ϵ) and the optical dielectric constant (ϵ'') can be determined by the following equations [49].

$$\epsilon = n^2 \quad (13)$$

$$\epsilon'' = n^2 - 1 \quad (14)$$

The obtained values of ϵ and ϵ'' are listed in Table 4, we notice that the values of permittivity ϵ , and the optical dielectric constant ϵ'' , increase with the increase in Bi_2O_3 content. Because Bi_2O_3 causes network defects, an increase in glass disordering and produces NBO, it acts as a modifier in the present glass network [42].

The optical electronegativity (χ^*) obtained from the formula [50]:

$$\chi^* = 2.688 E_g \quad (15)$$

The linear dielectric susceptibility ($\chi^{(1)}$) calculated from the formula [50]:

$$\chi^{(1)} = \frac{n^2 - 1}{4\pi} \quad (16)$$

The third-order nonlinear optical susceptibility (χ^3) determined by using the formula [51].

$$\chi^3 = \frac{A}{(4\pi)^4(n-1)^4} \quad (17)$$

Where $A = 1.7 \times 10^{-10}$ (for $\chi^{(3)}$ in esu). The values of linear dielectric susceptibility (χ^1) rises from 0.343 to 0.361 due to increment in NBOs and refractive index (n) with the addition of Bi_2O_3 content, while the other parameters optical electronegativity (χ^*) and nonlinear optical susceptibility (χ^3) are decreased from 9.028 to 8.520 and from 2.343×10^{-15} (esu) to 2.039×10^{-15} (esu) respectively. The dropping in the values of (χ^*) and (χ^3) is agreement with the drop in the values of the band gap when Bismuth content rises. NBOs increase in response to variations in the optical band gap (E_g), which is proportional to each of (χ^*) and (χ^3).

The relationship between the third-order nonlinear susceptibility χ^3 and the nonlinear refractive index (n_2), which depicts the interactions between intense electromagnetic radiations and different materials, is given by (n_2 expressed in esu) [51]:

$$n_2 = \left(\frac{2\pi}{n} \right) \chi^3 \quad (18)$$

The decreasing in the values n_2 in good agreement with the drop in the values of (χ^*), (χ^3), and the band gap energy and attributed to the increasing in NBOs.

3.4 Mechanical results

The elastic-mechanical factors were calculated by using the values of dissociation energy per unit volume (G_i) and packing density (PD) of the oxides according to Makishima–Mackenzie's theory [52]. The packing density was obtained by calculating the ratio of $\sum V_i x_i$ and V_m , where V_i is the packing factor for each chemical in the glass composite (determined by calculating the ionic radii of the components) and x_i represent the mole fraction, while V_m is the molar volume of the glass composite as shown in Table.5. The G_i of current glasses gradually increased from 33.26 to 33.58 kJ/cm³ when replacing PbO with Bi_2O_3 from 0 to 5 mol%, because the G_i of bismuth oxide is higher than that of lead oxide, as well as the packing factor of Bi_2O_3 (26.1 cm³/mol) is higher than the packing factor of PbO (11.1 cm³/mol).

From these values and mechanical equation in the above section, the elastic-mechanical moduli (Young's (E), bulk (K), shear (S), longitudinal (L)) were calculated and reported in Table.5 and plotted in Fig.14. The four moduli showed the same behavior, where the moduli values gradually increased with the replacement of PbO contents with Bi_2O_3 until the glassy composite Bi-3.0 (containing 3 mol% of Bi_2O_3 and 2 mol% of PbO) and it is gradually declined again. The main reason is the PD values equal 0.516, 0.518, 0.519, 0.519, 0.516 and 0.516 cm³/mol for Bi-0.0, Bi-1.0, Bi-2.0, Bi-3.0, Bi-4.0 and Bi-5.0, respectively. For example, the Young's modulus (E) values was 34.34, 34.50, 34.68, 34.75, 34.59 and 34.34 GPa, respectively, which means that adding the two oxides by equal proportion gives improving the mechanical properties of the sample. On the other hand, glass sample Bi-0.0 (which does not contain Bi_2O_3) gives almost the same elastic-mechanical properties as sample Bi-5.0 (which does not contain PbO). From Fig.14, it turned out that the lowest modulus of the four parameters was the shear modulus (S), where the highest values were for Bi-3.0, with 14.10 GPa, while the largest result was for the Young modulus, the maximum for the same glass sample was 34.75 GPa, followed by the longitudinal modulus with a maximum value of 32.23 GPa.

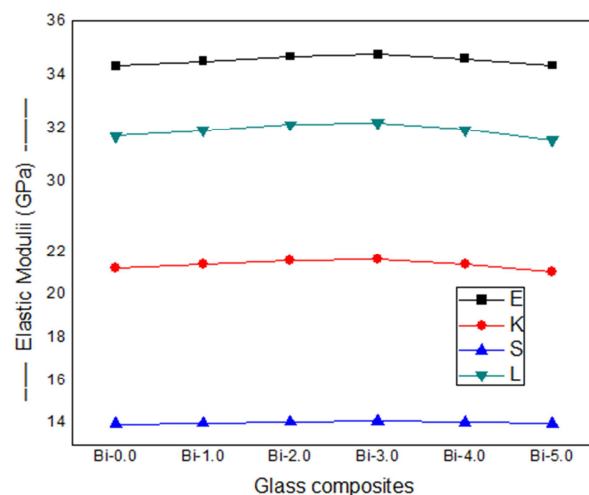


Figure 14: The elastic moduli (Young, Bulk, shear and longitudinal modulus) of the present glass composites.

Fig.15 indicates Poisson's ratio, whose value ranges from 0.231 to 0.233, meaning that there was a small change of 0.002. This means that the glass samples did not differ with the exchange during the elongation process, while the micro-hardness values gradually increase. This indicates that the samples will be harder with the replacement of PbO with Bi₂O₃, where their values range from 2.502 to 2.531 GPa, as shown in the Figure.

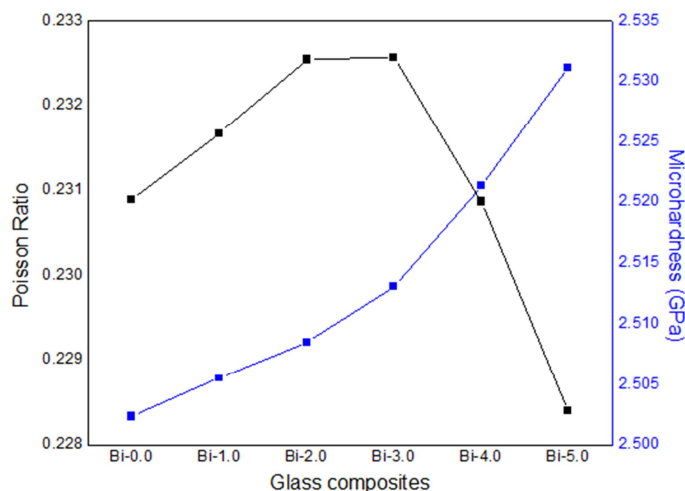


Figure 15: The Poisson ratio and the micro-hardness of the present glass composites.

Table 5: Mechanical results of Bi-0.0-Bi-5.0 coded glass composites.

Glass Code	V_m (cm ³ /mol)	E (GPa)	K (GPa)	S (GPa)	L (GPa)
Bi-0.0	26.32	34.34	21.27	13.95	31.73
Bi-1.0	26.53	34.50	21.43	14.01	31.93
Bi-2.0	26.7	34.68	21.61	14.07	32.16
Bi-3.0	27.02	34.75	21.66	14.10	32.23
Bi-4.0	27.4	34.59	21.42	14.05	31.96
Bi-5.0	28.03	34.34	21.08	13.98	31.56

4. Conclusions

The new glasses made of 70B₂O₃ - 5SiO₂ - 10Li₂O - (5-x)PbO - 10ZnO - xBi₂O₃, where x = 0.0:5 mol% are created using melt-quenching process. By replacing 5 mol% of PbO with Bi₂O₃, the density increased from 2.67 to 2.94 g/cm³. For the samples Bi-0.0, Bi-1.0, Bi-2.0, Bi-3.0, Bi-4.0, and Bi-5.0, the corresponding (MAC) values were 0.140, 0.147, 0.153, 0.159,

0.164, and 0.170 cm² g⁻¹. For Bi-0.0, Bi-1.0, Bi-2.0, Bi-3.0, Bi-4.0, and Bi-5.0, the corresponding TVL values at 0.05 MeV were 0.513, 0.458, 0.413, 0.378, 0.351, and 0.329 cm. When the amount of Bi³⁺ ions in the glass structure rose, the band gap of optical energy (directly as well as indirectly) reduced, but the Urbach energy increased due to structural defects in the resultant glass. It has also been demonstrated that increasing non-bridging oxygens (NBOs) by adding Bi³⁺ ions raise the dielectric constant (ϵ), optical dielectric constant (ϵ''), and index of refraction (n). The other optical characteristics, like χ^* , χ^3 , and n_2 optical, also decreased. When PbO contents were replaced with Bi₂O₃, mechanical moduli values gradually ascended until they reached the glassy composite Bi-3.0, which contains 2 mol% PbO and 3 mol% Bi₂O₃, at which point they gradually decreased once more.

5. Conflicts of interest

The authors declare that they have no conflict of interest.

6. Formatting of funding sources

7. Acknowledgments

This research project was funded by the Deanship of Scientific Research and Libraries, Princess Nourah bint Abdulrahman University, through the Program of Research Project Funding After Publication, grant No (RPFAP-104- 1445)

8. References and Bibliography

- [1] V. Agrawal, R. Paulose, R. Arya, G. Rajak, A. Giri, A. Bijanu, S.K. Sanghi, D. Mishra, N. Prasanth, A.K. Khare, V. Parmar, M.A. Khan, A. Bhisikar, A.K. Srivastava, S.T. Salammar, Green conversion of hazardous red mud into diagnostic X-ray shielding tiles, *J. Hazard. Mater.* 424 (2022) 127507. <https://doi.org/10.1016/j.jhazmat.2021.127507>
- [2] G.A. Alharshan, N.M. Ebrahim, M. Elsaifi, R.A. Elsad, A.M.A. Mahmoud, Y.I. Mesalam, S.A. Said, A. Mimouni, The Lanthanum-Doped Phosphate Glass System: Optical, Mechanical, and Gamma-Ray Shielding Properties. *J Inorg Organomet Polym* 35 (2025) 1397–1412 (2025). <https://doi.org/10.1007/s10904-024-03371-2>
- [3] G. A. Alharshan, A. M. A. El-Seidy, M.I. Elamy, I.M. Nabil, A.M. El-Refaey, R. A. Elsad, M. S. Shams, A. M. Abdelghany, Y. S. Rammah, CeO₂ additive to bismo-borate glasses: synthesis, structure, physical characteristics, and radiation protection competence. *J. Mater. Sci.: Mater. Electron.* 35(2024) 862 <https://doi.org/10.1007/s10854-024-12610-8>
- [4] F.A. Mettler, Medical effects and risks of exposure to ionizing radiation, *J. Radiol. Prot.* 32 (1) (2012) N9–N13, <https://doi.org/10.1088/0952-4746/32/1/N9>.
- [5] N.A.M. Alsaif, Z.Y. Khattari, M.S. Shams, Y.S. Rammah, A.M. El-Refaey, and R.A. Elsad, Elastic-mechanical, dielectric properties, and γ radiation safety competence of calcium boro-zinc glass systems reinforced with Nb⁵⁺ ions: experimental and theoretical studies. *J. Mater. Sci.: Mater. Electron* 34, (2023) 402. <https://doi.org/10.1007/s10854-023-09835-4>
- [6] G.A. Alharshan, M.I. Elamy, S.A. Said, A.M.A. Mahmoud, R.A. Elsad, I.M. Nabil, N.M. Ebrahim, Effect of lanthanum oxide on the radiation-shielding, dielectric, and physical properties of lithium zinc phosphate glasses. *Radiat. Phys. Chem.* 224(2024) 112053. <https://doi.org/10.1016/j.radphyschem.2024.112053>
- [7] B. Aygün, High alloyed new stainless steel shielding material for gamma and fast neutron radiation, *NUCL ENG TECHNOL* 52 (2020) 647–653 <https://doi.org/10.1016/j.net.2019.08.0>
- [8] B. Aygün, Neutron and gamma radiation shielding Ni based new type super alloys development and production by Monte Carlo Simulation technique. *Radiat. Phys. Chem.* 188 (2021): 109630. <https://doi.org/10.1016/j.radphyschem.2021.109630>
- [9] S.M. Shaaban, N.A.M. Alsaif, H. Al-Ghamdi, Z. Y. Khattari, Y. S. Rammah, A.M. El-Refaey, M.S. Shams, R.A. Elsad, Influence of Copper Ions on the Structural, Mechanical, Radiation Shielding and Dielectric Properties of Borate Zinc-Fluoride Glasses. *J. Electron. Mater.* 52(2023) 6269–6276. <https://doi.org/10.1007/s11664-023-10564-x>
- [10] N.A.M. Alsaif, Z.Y. Khattari, Y.S. Rammah, M.S. Shams, and R.A. Elsad, Bismo-borate glasses doped with La³⁺ and Eu³⁺ ions: synthesis, physical, optical and electrical characteristics. *J Mater Sci: Mater Electron* 33(2022) 19667–19677. <https://doi.org/10.1007/s10854-022-08803-8>
- [11] Y.S. Choi, S.M. Lee, Fundamental properties and radioactivity shielding performance of concrete recycled cathode ray tube waste glasses and electric arc furnace slag as aggregates, *Prog. Nucl. Energy* 133 (2021) 103649. <https://doi.org/10.1016/j.pnucene.2021.103649>
- [12] G. Tyagi, A. Singhal, S. Routroy, D. Bhunia, M. Lahoti, Radiation Shielding Concrete with alternate constituents: An approach to address multiple hazards, *J. Hazard. Mater.* 404 (2021) 124201. <https://doi.org/10.1016/j.jhazmat.2020.124201>
- [13] G.A. Alharshan, S.M. Shaaban, S.A. Said, A.M.A. Mahmoud, A.A. Altohamy, R.A. Elsad, N.M. Ebrahim, [Impact of Yttrium Oxide on the Dielectric, Radiation-Shielding, and Physical Characteristics of Glasses Made of Lithium Bismuth Zinc Phosphate](https://doi.org/10.1007/s10904-024-03461-1). *J Inorg Organomet Polym* (2024). <https://doi.org/10.1007/s10904-024-03461-1>
- [14] G.A. Alharshan, N.M. Ebrahim, S.M. Shaaban, S.A. Said, R.A. Elsad, A.A. Altohamy, Y.S. Rammah, F. Ibraheem, Manufacturing, Optical, Dielectric, and Gamma-Attenuation Characteristics of Phosphate Glasses Doped with Lanthanum and Erbium. *J Inorg Organomet Polym* (2024). <https://doi.org/10.1007/s10904-024-03441-5>

- [15] G. AlMisned, D. Sen Baykal, G. Kilic, G. Susoy, H.M. Zakaly, A. Ene, H.O. Tekin, Assessment of the usability conditions of $\text{Sb}_2\text{O}_3\text{-PbO-B}_2\text{O}_3$ glasses for shielding purposes in some medical radioisotope and a wide gamma-ray energy spectrum, *Appl. Rheol.* 32 (1) (2022) 178–189, <https://doi.org/10.1515/arh-2022-0133>.
- [16] Ahmed M Abdel-Aziz, RA Elsad, Emad M Ahmed, YS Rammah, MS Shams, MH Misbah, Synthesis, physical, ultrasonic waves, mechanical, FTIR, and dielectric characteristics of $\text{B}_2\text{O}_3/\text{Li}_2\text{O}/\text{ZnO}$ glasses doped with Y^{3+} ions, *J Mater Sci: Mater Electron* 33 (2022) 6603–6615. <https://doi.org/10.1007/s10854-022-07835-4>
- [17] A. Almuqrin, J.S Al-Otaibi, N. Alwadai, B. Albarzan, R.A. Elsad, M.S. Shams, Y.S. Rammah, Borosilicate glasses doped with Er_2O_3 : preparation, physical, optical, dielectric properties and radiation shielding capacity. *Appl. Phys. A* 130 (2024) 893. <https://doi.org/10.1007/s00339-024-08071-9>
- [18] M. Mariyappan, K. Marimuthu, M.I. Sayyed, M.G. Dong, U. Kara, Effect Bi_2O_3 on the physical, structural and radiation shielding properties of Er^{3+} ions doped bismuth sodium fluoroborate glasses, *J. Non. Cryst. Solids* 499 (2018) 75–85. <https://doi.org/10.1016/j.jnoncrysol.2018.07.025>
- [19] E.S.A. Waly, M.A. Fusco, M.A. Bourham, Gamma-ray mass attenuation coefficient and half value layer factor of some oxide glass shielding materials, *Ann. Nucl. Energy* 96 (2016) 26–30. <https://doi.org/10.1016/j.anucene.2016.05.028>
- [20] V.P. Singh, N.M. Badiger, and J. Kaewkhao, Radiation shielding competence of silicate and borate heavy metal oxide glasses: Comparative study, *J. Non. Cryst. Solids* 404 (2014) 167–173. <https://doi.org/10.1016/j.jnoncrysol.2014.08.003>
- [21] Material explorer/Bi-O/ Bi_2O_3 / mp-23262, [mp-23262: Bi2O3 \(Monoclinic, P2_1/c, 14\) \(materialsproject.org\)](https://doi.org/10.26434/chemrxiv-2020-04-14)
- [22] Materials Data on PbO by Materials Project (Dataset) | DOE Data Explorer (osti.gov), 29 April 2020, <https://doi.org/10.17188/1281794>.
- [23] E.S.A. Waly, M.A. Fusco, and M.A. Bourham, Gamma-ray mass attenuation coefficient and half value layer factor of some oxide glass shielding materials, *Ann. Nucl. Energy* 96 (2016) 26–30. <https://doi.org/10.1016/j.anucene.2016.05.028>
- [24] M. Kurudirek, N. Chutithanapanon, R. Laopaiboon, C. Yenchai, C. Bootjomchai, Effect of Bi_2O_3 on gamma ray shielding and structural properties of borosilicate glasses recycled from high pressure sodium lamp glass, *J. Alloys Compd.* 745 (2018) 355–364. <https://doi.org/10.1016/j.jallcom.2018.02.158>
- [25] H.D. Shashikala, and N.K. Udayashankar, Influence of Fe^{3+} ions on optical, structural, thermal and mechanical properties of $\text{Li}_2\text{O-Na}_2\text{O-K}_2\text{O-ZnO-B}_2\text{O}_3$ based glass system, *Ceram. Int.* 46(4) (2020) 5213–5222. <https://doi.org/10.1016/j.ceramint.2019.10.269>
- [26] M. Mariyappan, K. Marimuthu, M.I. Sayyed, M.G. Dong, and U. Kara, Effect Bi_2O_3 on the physical, structural and radiation shielding properties of Er^{3+} ions doped bismuth sodium fluoroborate glasses, *J. Non. Cryst. Solids* 499 (2018) 75–85. <https://doi.org/10.1016/j.jnoncrysol.2018.07.025>
- [27] Erdem Şakar, Özgür Fırat Özpolat, Bünyamin Alım, M.I. Sayyed, Murat Kurudirek. Phy-X / PSD: Development of a user friendly online software for calculation of parameters relevant to radiation shielding and dosimetry. *Radiat. Phys. Chem.* 166 (2020) 108496. <https://doi.org/10.1016/j.radphyschem.2019.108496>
- [28] J.F. Briesmeister, MCNP[^]-A General Monte Carlo N-Particle Transport Code, Version 4C, LA-13709-M. (2000).
- [29] M.S. Badawi, S. Noureddine, Y.N. Kopatch, M.I. Abbas, I.N. Ruskov, D.N. Grozdanov, A.A. Thabet, N.A. Fedorov, M.M. Gouda, C. Hramco, others, Characterization of the efficiency of a cubic NaI detector with rectangular cavity for axially positioned sources, *J. Instrum.* 15 (2020) P02013. DOI 10.1088/1748-0221/15/02/P02013
- [30] A.M.A. El-Seidy, O.I. Sallam, I.M. Nabil, Y.S. Rammah, M.S. El-Okkaily, H. Alshater, Preparation, physical, optical, ESR and γ -ray attenuation efficacy investigation of copper oxide/silver borosilicate glass. *Sci Rep* 14 (2024) 25354. <https://doi.org/10.1038/s41598-024-75017-9>
- [31] O.I. Sallam, Y.S. Rammah, I.M. Nabil, A.M.A. El-Seidy, Enhanced optical and structural traits of irradiated lead borate glasses via Ce^{3+} and Dy^{3+} ions with studying Radiation shielding performance. *Sci Rep* 14 (2024) 24478. <https://doi.org/10.1038/s41598-024-73892-w>
- [32] B. Speit, Radiation-shielding Glasses Providing Safety Against Electrical Discharge and Being Resistant to Discoloration, 1991 Google Patents.
- [33] M. Elsafi, A.M. Hedaya, M.I. Sayye. Study the impact of MgO , Al_2O_3 , MoO_3 , BaO , ZnO and PbO on the radiation shielding performance of borate glasses. *Nucl. Eng. Technol.* 57 (2025) 103475 <https://doi.org/10.1016/j.net.2025.103475>
- [34] E. Ebrahimi, M. Rezvani, Optical and structural investigation on sodium borosilicate glasses doped with Cr_2O_3 , *Spectrochim Acta Part A Mol. Biomol. Spectrosc.* 190 (2018) 534–538 <https://doi.org/10.1016/j.saa.2017.09.031>
- [35] G. Chandrashekaraiyah, N.S. Reddy, B. Sujatha, R. Viswanatha, C. Narayana Reddy, Role of Er^{3+} and Bi^{3+} ions on thermal and optical properties of $\text{Li}_2\text{B}_4\text{O}_7$ glasses: structural correlation. *J. Non. Cryst. Solids* 498 (2018) 252–261 <https://doi.org/10.1016/j.jnoncrysol.2018.06.034>
- [36] I. Kashif, A. Ratep, Optical properties of borate glasses containing chromium and erbium oxide, *Appl. Phys. A* 129 (2023) 489 <https://doi.org/10.1007/s00339-023-06764-1>
- [37] N.F. Mott, E.A. Davis, *Electronic Processes in Non-crystalline Materials*, second ed., Oxford University Press, Oxford, 1977.
- [38] E.A. Davis, N.F. Mott, Conduction in non-crystalline systems conductivity, optical absorption and photoconductivity in amorphous semiconductors. *Philos. Mag.* 22 (1970) 903–922 <https://doi.org/10.1080/14786437008221061>
- [39] I. Bulus, M. Isah, M.E. Garba, R. Hussin, S.A. Dalhatu, Influence of Eu^{3+} Dopant on Physical and Optical Properties of Lithium-Borosulfophosphate Glasses, *Niger. J. Technol. Dev.* 15(4) (2018) 121–127 doi: <http://dx.doi.org/10.4314/njtd.v15i4.3>
- [40] F. Urbach, The long-wavelength edge of photographic sensitivity and of the electronic absorption of solids. *Phys. Rev.* 92 (1953) 1324 <https://doi.org/10.1103/PhysRev.92.1324>

- [41] S.H. Alazoumi, S.A. Aziz, R. El Mallawany, U. Sa'ad Aliyu, H.M Kamari, M. H.M. Zaid, K.A. Matori, A. Ushah, Optical properties of zinc lead tellurite glasses, *Results Phys.* 9 (2018) 1371–1376 <https://doi.org/10.1016/j.rinp.2018.04.041>
- [42] O. Bawazeer, Structural, optical, and shielding properties of lead borate glasses doped with copper oxide, *Mater. Res. Express* 11 (2024) 015201 DOI 10.1088/2053-1591/ad19b2
- [43] V.P. Singh, M.E. Medhat, N.M. Badiger, Photon attenuation coefficients of thermoluminescent dosimetric materials by Geant4 toolkit, XCOM program and experimental data: a comparison study, *Ann. Nucl. Energy* 68 (2014) 96–100 <https://doi.org/10.1016/j.anucene.2014.01.011>
- [44] K. Annapoorani, C.H. Basavapoornima, N. Suriya Murthy, K. Marimuthu, Investigations on structural and luminescence behavior of Er^{3+} doped Lithium Zinc borate glasses for lasers and optical amplifier applications, *J. Non-Cryst. Sol.* 447 (2016) 273–282 <https://doi.org/10.1016/j.jnoncrsol.2016.06.021>
- [45] X. Zhao, X. Wang, H. Lin, Z. Wang, A new approach to estimate refractive index, electronic polarizability, and optical basicity of binary oxide glasses, *Physica B* 403 (2008) 2450–2460 <https://doi.org/10.1016/j.physb.2008.01.009>
- [46] M.I. Sayyed, M. Rashad, Y.S. Rammah, Impact of Ag_2O on linear, nonlinear optical and gamma-ray shielding features of ternary silver vanadio-tellurite glasses: $\text{TeO}_2\text{--V}_2\text{O}_5\text{--Ag}_2\text{O}$, *Ceram. Int.* 46 (2020) 22964–22972 <https://doi.org/10.1016/j.ceramint.2020.06.071>
- [47] G. Lakshminarayana, S.O. Baki, A. Lira, M.I. Sayyed, I.V. Kityk, M.K. Halimah, M.A. Mahdi, X-ray photoelectron spectroscopy (XPS) and radiation shielding parameters investigations for zinc molybdenum borotellurite glasses containing different network modifiers, *J. Mater. Sci.* 52 (2017) 7394–7414 <https://doi.org/10.1007/s10853-017-0974-0>
- [48] V. Dimitrov, T. Komatsu, Electronic polarizability, optical basicity and nonlinear optical properties of oxide glasses. *J. Non-Cryst. Solids* 249 (1999) 160–179 [https://doi.org/10.1016/S0022-3093\(99\)00317-8](https://doi.org/10.1016/S0022-3093(99)00317-8)
- [49] T.Y. Lim, H. Wagiran, R. Hussin, S. Hashim, M.A. Saeed, Physical and optical properties of dysprosium ion doped strontium borate glasses, *Physica B* 451 (2014) 63–67 <https://doi.org/10.1016/j.physb.2014.06.028>
- [50] J.A. Duffy, *Bonding, Energy Level and Bonds in Inorganic Solids*, Longman, England, 1990.
- [51] H. Ticha, L. Tichy, Semiempirical relation between non-linear susceptibility (refractive index), linear refractive index and optical gap and its application to amorphous chalcogenides, *J. Optoelectron. Adv. Mater.* 4 (2002) 381–386.
- [52] A. Makishima, J.D. Mackenzie, Direct calculation of Young's modulus of glass, *J. Non-Cryst. Solids* 12 (1973) 35–45. [https://doi.org/10.1016/0022-3093\(73\)90053-7](https://doi.org/10.1016/0022-3093(73)90053-7)